BRILL

IAWA Journal 46 (4), 2025: 551-566

iawa

High-resolution imaging of the physical and chemical properties of *Populus* wood using SilviScan™ and near-infrared spectroscopy

Anna Renström [1,*], Gerhard Scheepers [2,*], Zakiya Yassin [2], Thomas Grahn [2], Pramod Sivan [1], Totte Niittylä [1], Ewa J. Mellerowicz [1] and Hannele Tuominen [1]

[1] *Umeå Plant Science Centre, Department of Forest Genetics and Plant Physiology, Swedish University of Agricultural Sciences, SE-901 87, Umeå, Sweden*
[2] *RISE Research Institutes of Sweden AB, Box 857, 501 15, Borås, Sweden*
**Corresponding authors; emails: anna.renstrom@slu.se; gerhard.scheepers@ri.se*
ORCID iDs: Renström: 0009-0004-8104-3228; Scheepers: 0000-0002-5630-1377; Yassin: 0000-0001-6878-3361; Grahn: 0000-0001-5287-3629; Sivan: 0000-0001-5297-2221; Niittylä: 0000-0001-8029-1503; Mellerowicz: 0000-0001-6817-1031; Tuominen: 0000-0002-4949-3702

Accepted for publication: 31 January 2025; published online: 14 February 2025

Summary – Spatial information on wood structure and chemistry is crucial for understanding wood functionality. We present a high-throughput and high-resolution near-infrared (NIR) method for combined imaging of the physical and chemical properties of stem sections from *Populus* trees. Pyrolysis-GC/MS data was used for sensitive and spatially resolved calibration of wood chemistry while SilviScan™ analyses provided reference data for wood physical properties with 25 µm resolution for wood density and 0.2–2.0 mm for microfibril angle (MFA). NIR prediction models were trained and calibrated on material from both field- and greenhouse-grown trees. Thus, the method was developed for NIR imaging of stem samples as small as 4 mm in diameter with an image resolution of 0.03 mm for small-diameter samples and 0.5 mm for samples with multiple annual rings. The NIR model performance, tested against data not used in the training set, reached the coefficient of determination (R^2_{pred}) values for wood density and MFA of 0.60 and 0.72, respectively. The NIR models for wood chemistry showed R^2_{pred} values of 0.78 and 0.77 for carbohydrates and lignin, respectively. Models for the G-, S- and H-type lignin had R^2_{pred} values between 0.58 and 0.86. In addition, we developed a prediction model for the determination of tension wood distribution. According to this model, tension wood was frequently observed in young greenhouse samples, which might explain the higher variation found in the chemical and physical properties of wood in greenhouse-grown compared to field-grown trees. The study also demonstrated that NIR-model estimations in image format can capture spatial variations that are not detectable in bulk analyses of wood properties. Examples of the method applied to greenhouse-grown trees highlight the efforts to develop NIR models with good prediction accuracies based on high-resolution data.

Keywords – NIR-imaging, NIR prediction models, Py-GC/MS, SilviScan, wood chemistry, wood properties.

Introduction

Near-infrared (NIR) spectroscopy is based on the reflectance or transmittance of electromagnetic waves in the near-infrared region (800–2500 nm). The resulting spectra show the interaction between the analyzed material and the light. The technique is non-destructive, fast, and requires minimal sample preparation. NIR spectroscopy, combined with calibration and multivariate analysis, has therefore been used as a tool to characterize wood and wood material on both a quantitative and qualitative level. Most recent advances in the field involve NIR hyperspectral imaging, which combines spectra and image processing to provide additional spatial determination (Tsuchikawa 2007; Hein *et*

© The authors, 2025
This is an open access article distributed under the terms of the CC BY 4.0 license.

DOI 10.1163/22941932-bja10179

al. 2017). High-resolution physical characterization with a combination of NIR spectroscopy and SilviScan™ reference measurements has been applied previously to various wood samples for the determination of wood density, fiber length, microfibril angle, and other physical properties (Schimleck *et al.* 2005; Mora & Schimleck 2009; Inagaki *et al.* 2012; Cieszewski *et al.* 2013; Giroud *et al.* 2017). Whole-tree mapping of physical properties was demonstrated with NIR by taking increment cores at different tree heights using SilviScan™ data as reference data (Mora & Schimleck 2009; Schimleck *et al.* 2018). Morphological wood traits, such as cell wall thickness, were modeled with NIR using SilviScan™ reference data in *Pinus taeda* (Isik *et al.* 2011). A more recent study focused on the physical properties of transverse profiles of wood from various tree species, using NIR fibre optic point measurements with a 2-mm resolution and SilviScan™ as a reference method (Giroud *et al.* 2021). However, models based on NIR images of wood have not been described with a resolution below 2 mm, which would be especially important for trees with small diameters.

Reference data for wood chemical characterization with NIR is often based on wet chemistry extraction methods of bulk tissues (Jones *et al.* 2006; Poke & Raymond 2006; Thumm *et al.* 2016; Fahey *et al.* 2019). Even though such reference methods have been useful, they cannot provide sufficient spatial resolution for the calibration of the NIR data. Precise chemical information over a wood transverse section requires a sensitive method that allows the analysis of small sample sizes. Analytical Pyrolysis-Gas Chromatography/Mass Spectrometry (Py-GC/MS) has the advantage of minimal sample preparation and requires only 5–200 μg of material (Kusch 2018). Hence, this method can provide chemical reference data with a similar spatial resolution to the NIR scans. Even though analytical pyrolysis is a semi-qualitative method, a good correlation was demonstrated between Klason lignin and pyrolysis-lignin in *Eucalyptus* spp. (Alves *et al.* 2021). In addition, a close correlation was shown between Py-GC/MS and nuclear magnetic resonance (NMR) data in *Populus* spp. (Karmanov *et al.* 2023; Renström *et al.* 2024). These attributes establish Py-GC/MS as an attractive tool for acquiring precise reference data for spatial NIR models.

SilviScan™ technology (Evans 1994) is usually applied to field-grown forest trees with large stem diameters and multiple annual rings, and there are only a few examples of the application of SilviScan™ to greenhouse samples. Notable exceptions are the studies from Erasmus *et al.* (2020) where *ca.* 15 mm diameter greenhouse-grown *Pinus* spp. seedlings were analyzed for the effects of drought and fertilization, and recent greenhouse studies in *Populus* trees (Escamez *et al.* 2017, 2023; Urbancsok *et al.* 2023). However, there is a demand for large-scale characterization of greenhouse samples. The physical and chemical characterization of small samples can be cumbersome. In this work, we report on an efficient pipeline, enabled by the simultaneous scan with NIR and SilviScan™, for high-resolution imaging of chemical and physical properties of transverse wood discs in *Populus* stems as small as 4 mm in diameter.

Materials and methods

Sample preparation and NIR imaging

Stem samples from approx. 2-months-old greenhouse-cultivated hybrid aspen (*Populus tremula* L. × *P. tremuloides* Michx.) trees with a diameter of 4–10 mm were trimmed to a length of 13 ± 1 mm and glued to a high-density fiberboard (HDF) base (Fig. 1A). Samples were dried either before or after the trimming. This was followed by sanding the transverse surfaces consecutively with 400, 600, 800, and finally 1200 grit sandpaper to the same height before scanning with a NIR line camera (Specim ImSpector N25E) fitted over a conveyor belt. The scanning was done at 0.03 mm resolution (the highest resolution possible) with 256 steps in the 900–2500 nm wavelength range. As an object passed by the camera, a hyperspectral image was built up yielding a final image dimension of 360 pixels perpendicular to the feeding direction and as many pixels as desired along the feeding direction. Since the reflectance or absorbance was measured at 256 wavelength bands, each hyperspectral image consisted of 256 stacked images with 256 values at each pixel. For comparison, a normal RGB image has three values per pixel, one for each wavelength band representing red, green or blue.

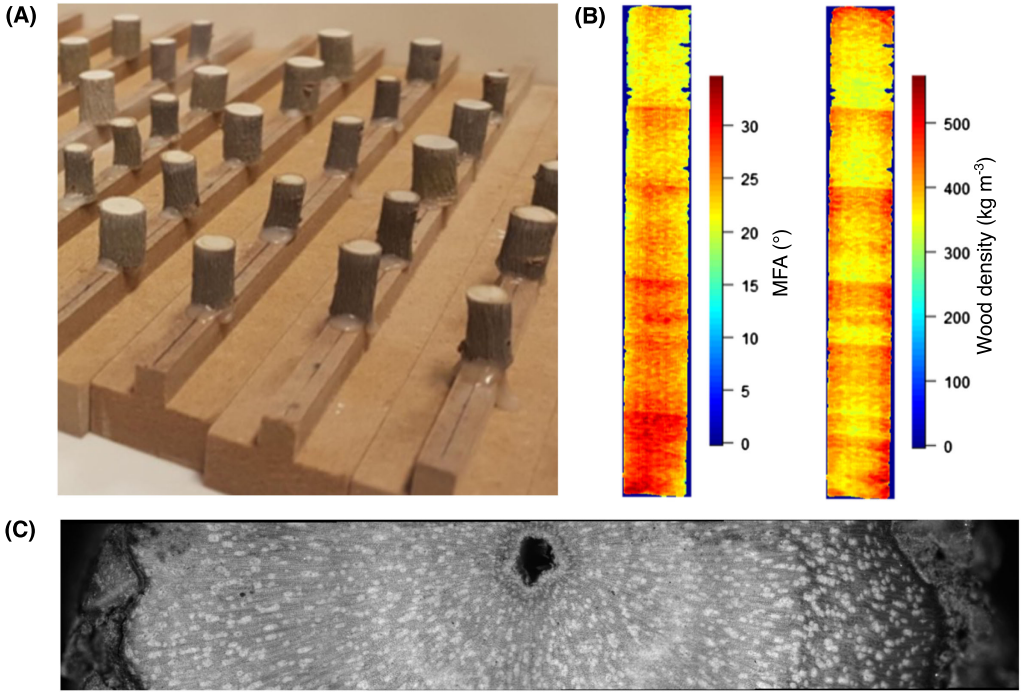

Fig. 1. Sample preparation and high-resolution NIR imaging for the NIR models. (A) The preparation pipeline of small-diameter stems. Stem samples, 4–10 mm in diameter, were collected from greenhouse-grown trees. The samples were cut to a length of 13 ± 1 mm and glued to the high-density fiberboard (HDF) bases. This was followed by a surface polish, where the samples were sanded to have the same level before scanning with the NIR line camera and the subsequent production of SilviScan™ samples. (B) Prediction of microfibril angle (MFA) and wood density of a SilviScan™ sample. Samples were scanned with NIR at 0.03-mm resolution on the transverse surface of a SilviScan™ sample collected from a field-grown tree. Images were processed using a 5 × 5-pixel median filter to reduce noise (see Materials and Methods). (C) A stitched microscopy image with 1.29 μm resolution of the transversal area of a SilviScan sample.

Wood discs were collected from approx. 6–10 year-old, field-grown aspen (*Populus tremula* L.) trees with a stem diameter of approx. 5–10 cm, and were trimmed to a disc thickness of 15 ± 1 mm. The wood discs were cut in the vertical direction with a bandsaw from the bark to the pith to avoid uncontrolled cracking when dried at room temperature. The dry discs were then sanded, as described for greenhouse samples, on the transverse surfaces and scanned with the same NIR line camera, but at a lower resolution (0.5 mm), to accommodate the larger diameter of the field-grown samples in a wider optical field of view. The lower resolution helps to shorten the time it takes to scan a larger sample. For the method to be considered high throughput, scanning times for both small and large samples were kept similar. SilviScan™ samples (width 2 mm, longitudinal height 7 mm, length from bark to pith) from field-grown trees were NIR scanned also at 0.03-mm resolution (Fig. 1B).

SilviScan™: wood physical properties

After NIR scanning, samples from the greenhouse-grown trees were trimmed to a width of 2 mm while still glued to the HDF base. These samples were trimmed and sanded to 7 mm longitudinal height and scanned on the transverse surfaces with the SilviScan™ cell scanner microscope at 1.3 μm resolution (for capturing wood morphology), the X-ray densitometer at 25 μm resolution (for measurement of wood density), and the X-ray diffractometer (for measurement of microfibril angle) at 0.2 mm resolution from bark-to-bark. For a detailed description of the SilviScan™ measurement

principles, see Cieszewski *et al.* (2013). The microscopy images were stitched without any loss of resolution according to the method of Preibisch *et al.* (2009) and applied in the FIJI open-source image processing software (Schindelin *et al.* 2012), version 2.14.0/1.54f (Fig. 1C). The lower tree diameter limit to produce satisfactory SilviScan™ samples was approximately 4 mm for dried and bark-free samples. Smaller diameter samples were difficult to handle since a radius below 2 mm interfered with the densitometry and X-ray diffraction measurements across the 2-mm-wide SilviScan™ sample.

Samples from the field-grown trees were prepared and scanned in the same way as the greenhouse samples but taken from the bark to the pith on the northern-facing side of the stem. For these samples, the X-ray densitometer was set to 25 μm resolution, the X-ray diffractometer to 2 mm resolution, and the microscopy images were taken at 1.3 μm resolution.

Pyrolysis-GC/MS: wood chemical composition

Pyrolysis-GC/MS was used to provide reference data on wood chemistry to the NIR models. In total, 300 samples from 40 field- and 80 greenhouse-grown trees were analyzed by Py-GC/MS. The 300 samples were obtained as a powder after drilling (in the longitudinal direction) at specific sites on the wood discs with a 1.5 mm diameter drill, which allowed precise spatial alignment of the data from Py-GC/MS and NIR. The aim was to include as much variation as possible in reference sampling for wood chemistry. Samples were acquired from areas in the transverse section that would not detriment the subsequent preparation of the SilviScan™ samples. Thus, the chemistry samples were collected after NIR scanning and before the preparation of the SilviScan™ sample.

Duplicate, 50 ± 10 μg wood powder samples were applied to a pyrolyzer equipped with an autosampler (PY-2020iD and AS-1020E, Frontier Lab, Fukushima, Japan) connected to a GC/MS (7890A/5975C; Agilent Technologies, Santa Clara, CA, USA). The method provided data on the relative contents of lignin, lignin subunits (syringyl (S), guaiacyl (G), *p*-hydroxyphenyl (H)) and carbohydrates (Gerber *et al.* (2012). The relative lignin content was calculated as the sum of the G (guaiacyl-type lignin), S (syringyl-type lignin), H (*p*-hydroxyphenyl-type lignin) and P (generic benzene derivatives without –OH group on the aromatic ring, most probably originated from lignin) fractions. The P fraction percentage varied between instrument runs and, consequently, only samples where the P fraction fell within the range of 0.6–1.2% were used for calibration of the NIR models. Altogether, Py-GC/MS data from 200 samples were used, and the average values of the duplicate measurements were spatially matched with the corresponding NIR spectra to create the multivariate NIR models.

NIR-models

The linear PLS (Partial Least Squares) models for different wood properties were trained on a random selection of 70% of the data and tested on the rest with the help of the multivariate data analysis tool Evince (Prediktera, Umeå, Sweden). The segmentation of wood and estimation of wood properties across the transverse area of the samples from the field-grown trees was conducted with the software Breeze (Prediktera). The wood physical and chemical properties of the sample surface were then estimated at 0.03 mm or 0.5 mm resolution, depending on the sample type (greenhouse or field-grown sample). The data from the SilviScan™ sample were overlayed with a best-fit algorithm with the NIR images for the evaluation of model performance in different sample types (Fig. 2).

A subset of field-grown trees was stimulated to induce the formation of tension wood, by mechanical bending of the trees in their last year of growth before harvesting. This material was then used to construct NIR models to determine tension wood distribution in samples. To provide reference data for the NIR models, the density and microfibril angle (MFA) data from SilviScan™ and the cell-scanner (microscopy) images were compiled to identify tension wood. The NIR spectra of the areas of wood with lower than normal (<15°) MFA and higher than normal (>500 kg/m^3) density were associated with tension wood and scored as probabilities from 0-1. These areas were also confirmed by light and scanning electron microscopy of the samples.

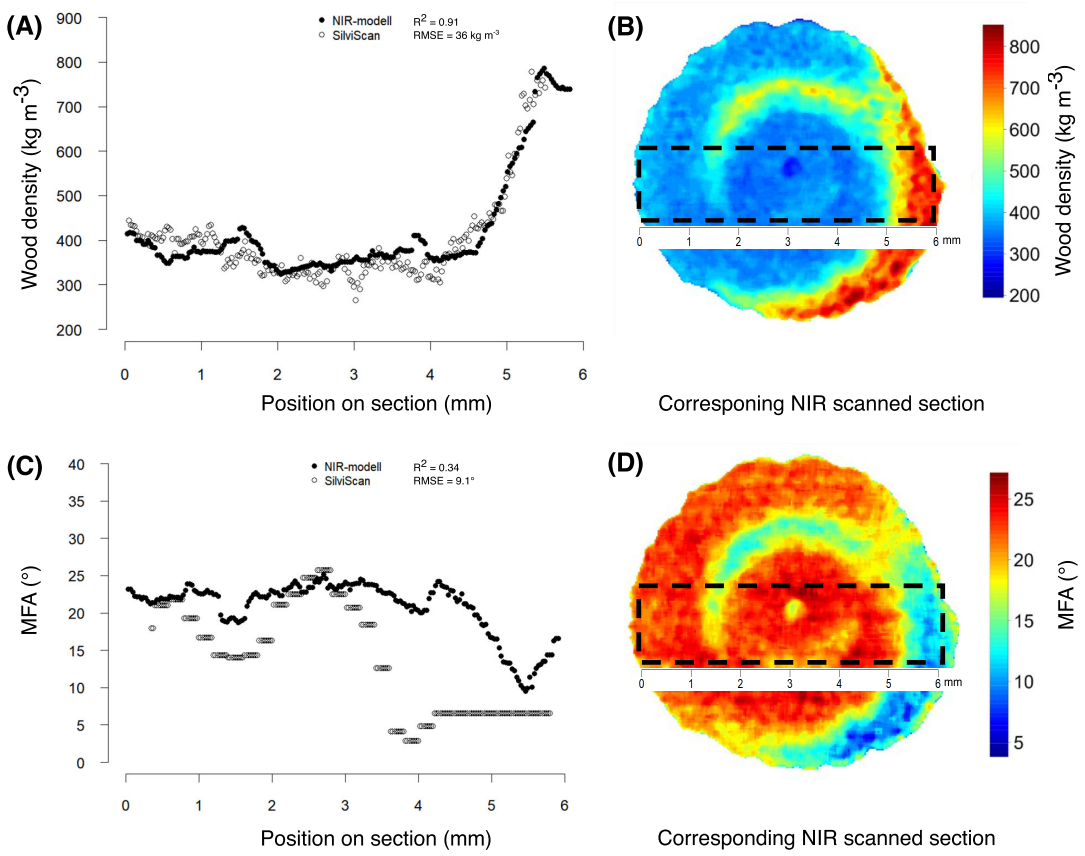

Fig. 2. An example of the manual overlay of data from a transverse SilviScan™ sample with the corresponding NIR image to evaluate the NIR model predictions. Values closest in distance to each other in the NIR image and the SilviScan™ sample were used to calculate the coefficient of determination R^2, and root mean square error RMSE. (A) Comparison of SilviScan™ measured wood density and the closest NIR prediction value using a best-fit algorithm. R^2 = 0.91, RMSE = 36 kg/m^3. (B) NIR predicted wood density map. (C) Comparison of SilviScan™ measured microfibril angle (MFA) and the closest NIR predicted value using a best-fit algorithm. R^2 = 0.34, RMSE = 9.1°. SilviScan™ produced false MFA values in the last ca. 1.5 mm of the section, and the NIR prediction reflected the variability at this position better. The algorithm to fit the NIR and the SilviScan™ data could not compensate for the error. (D) NIR predicted MFA map. The rectangular region in (B) and (D) shows the position of the SilviScan™ sample.

Image processing and statistics

Image processing, data analysis, graphs, and statistical testing were prepared using R studio (2023.12.1+402) and R version 4.3.1. NIR models were applied to either the raw images or 5 × 5-pixel median filtered images. The median filter was applied using the medianFilter function from EBImage package, which uses the median value for a 5 × 5 pixel area. Linear regressions, coefficient of determination (R^2), and root mean square error (RMSE) values were calculated using the functions; stat_poly_line(), stat_poly_eq() (ggpmisc package), and summarized() (dplyr package). Statistical tests included ANOVA (res_aov function) followed by Tukey's Post Hoc test (tukeyHSD function) and Wilcoxon rank sum test.

Wood property analysis of transverse sections versus bulk samples

The material and the experiments are described in detail by Renström *et al.* (2024). In short, approximately 2-month-old greenhouse-cultivated hybrid aspen trees (*Populus tremula* L. × *P. tremuloides* Michx.) were collected for wood characterization after being subjected to different nitrogen treatments. Transverse sections of the stems were NIR scanned, and 10-cm-long stem pieces, collected directly above the transverse section, were milled and analyzed for bulk wood chemistry by Py-GC/MS (Table A1 at 10.6084/m9.figshare.28322243). Wood density of bulk samples was measured using the water displacement method.

Results and discussion

NIR models for wood density and MFA

NIR models for wood density and MFA were constructed based on the NIR scans of the wood transverse surfaces at 0.03 mm resolution after calibration with the corresponding data from the SilviScan™ analysis of the same samples. This yielded approximately 4000 reference data points of which a random selection of 70% was used for model training and the rest for testing. The strength of the NIR models was evaluated by calculating the Root Mean Square Error of Prediction (RMSEP), which represents the accuracy of the predicted values (Faber, 1999), and R^2_{pred}, which is the coefficient of determination between the training set and a test set of data (Table 1). The proportion of the variance explained by the models, R^2_{pred} values were 0.60 for wood density and 0.72 for MFA. These values are comparable to earlier studies. Giroud *et al.* (2021) reported R^2_{pred} values 0.57–0.65 for wood density and 0.56–0.82 for MFA for NIR models that were based on data from a variety of tree species from mature stands. Mesquita Pimenta *et al.* (2024) obtained R^2_{pred} values 0.66–0.78 for wood density in *Eucalyptus* species, and Hein (2012) obtained R^2_{pred} values 0.71–0.75 for MFA, although the latter was measured on the radial surface.

Next, we investigated various factors, such as NIR resolution (0.5 or 0.03 mm), sample type (greenhouse or field samples), and image processing (with or without applied median filter; see Materials and methods), that could influence the accuracy of the NIR models for wood density and MFA. To evaluate the NIR models, we wanted to calculate the correlation between the values predicted by the model and those provided by the reference method. For this purpose, the values closest in proximity to each other in the NIR and SilviScan images were used to calculate the Pearson's correlation coefficient (R^2) in 18 randomly selected samples for each condition (Table 2; Fig. 2). Since

Table 1. The performance of NIR models for different chemical and physical characteristics. NIR models were tested against data not used in the training set.

Model	R^2_{pred}	RMSEP	Mean	SD	Data range (min–max)
Carbohydrates	0.78	2.13%	72.1%	4.6%	58.0–80.1%
Lignin	0.77	1.81%	24.6%	4.4%	17.2–38.4%
Syringyl units	0.58	1.55%	14.1%	2.5%	9.5–22.4%
Guaiacyl units	0.74	0.81%	8.5%	2.0%	5.2–15.3%
S:G ratio	0.66	0.16	1.70	0.32	1.2–2.8
p-hydroxyphenyl units	0.86	0.40%	1.23%	0.98%	0.34–3.46%
Wood density	0.60	129 kg/m^3	431 kg/m^3	90 kg/m^3	214–746 kg/m^3
MFA	0.72	5.0°	25.0°	3.8°	7.8–33.1°

R^2_{pred} is the coefficient of determination that shows the correlation between the predicted values of the NIR model and the reference data at the time of modeling. RMSEP is the root mean square error of prediction and shows the uncertainty that is introduced by the model. A representation of the whole data set is shown by mean values, SD and the full data range (min–max).

Table 2. The performance of the NIR MFA and wood density models compared to the measurements with SilviScan™.

Sample type	Resolution	Image processing	R^2_{mean}	R^2_{SD}	R^2_{min}	R^2_{max}	Tukey
MFA							
Field	0.5	5 × 5 median	0.53	0.29	0.01	0.94	a
Field	0.03	Raw	0.48	0.31	0.00	0.95	a
Field	0.03	5 × 5 median	0.47	0.30	0.00	0.95	a
Field	0.5	Raw	0.43	0.27	0.00	0.86	a
Greenhouse	0.03	5 × 5 median	0.34	0.31	0.02	0.91	a
Greenhouse	0.03	Raw	0.26	0.22	0.02	0.72	a
Wood density							
Greenhouse	0.03	5 × 5 median	0.68	0.20	0.15	0.97	a
Greenhouse	0.03	Raw	0.57	0.26	0.07	0.91	a
Field	0.5	5 × 5 median	0.35	0.12	0.16	0.54	b
Field	0.03	Raw	0.27	0.12	0.05	0.58	bc
Field	0.03	5 × 5 median	0.25	0.17	0.01	0.60	bc
Field	0.5	Raw	0.18	0.06	0.06	0.33	c

The R^2 value was calculated from the estimated position of the SilviScan™ measurement within each transverse section compared to the closest NIR prediction point using a best-fit algorithm. For evaluation purposes, samples were included from trees grown in the greenhouse and the field. The NIR scans were performed at 0.5 and 0.03 mm resolution and images were processed with or without an applied median filter. The statistical significance between the R^2 values was tested with ANOVA and Tukey's Post Hoc test, with different letters (in the "Tukey" column) indicating statistically significant differences. $\alpha = 0.05$, $n = 18$.

the NIR and SilviScan™ measurements were done with different resolutions, a complete match of data points was not possible, and a best-fit algorithm was used for the overlay.

For MFA, the highest correlation (R^2), 0.53, was shown for field samples scanned at 0.5 mm resolution. The R^2 values differed between the different sample types, but not in a statistically significant manner, which demonstrates that the model accuracy did not depend on NIR resolution, image processing, or sample type. However, the model showed a trend of better MFA prediction in field samples compared to greenhouse samples (Table 2). The 5 × 5-pixel median image filter applied to reduce unnecessary noise in the NIR images slightly improved the model performance while preserving the R^2_{SD} between the samples (Table 2).

For wood density, R^2 values ranged from 0.57 to 0.68 for greenhouse samples and from 0.18 to 0.25 for field samples (Table 2). Thus, the NIR model predicted wood density variations more accurately in the greenhouse samples. Similar to the MFA model, there was a trend of increased prediction accuracy with the applied image filter and no dependency on the NIR scan resolution (Table 2). We could therefore conclude that the lower NIR scan resolution of 0.5 mm did not affect the prediction quality and that image filtering slightly improved model prediction by reducing the noise. The wood density and MFA models generally performed better in the test set (Table 1) than in separate sets of samples containing either greenhouse- or field-grown samples (Table 2). The better performance in the test set is likely due to a higher overall variability in the data.

To explore the reason for differences in wood density model performance between the greenhouse and field samples, we analyzed whether the correlation depended on the variation within each sample (Fig. 3). In greenhouse samples, there was a clear linear relationship between R^2 values and within-sample variation for both wood density and MFA, demonstrating that variation in the trait influenced the prediction performance in this type of samples (Fig. 3A–B). In field samples, the model performance was less dependent on the within-sample variation than in the greenhouse samples; while the wood density model showed a slight correlation, the MFA model showed no correlation with the variation in the sample (Fig. 3A–B). An important difference between the field and greenhouse

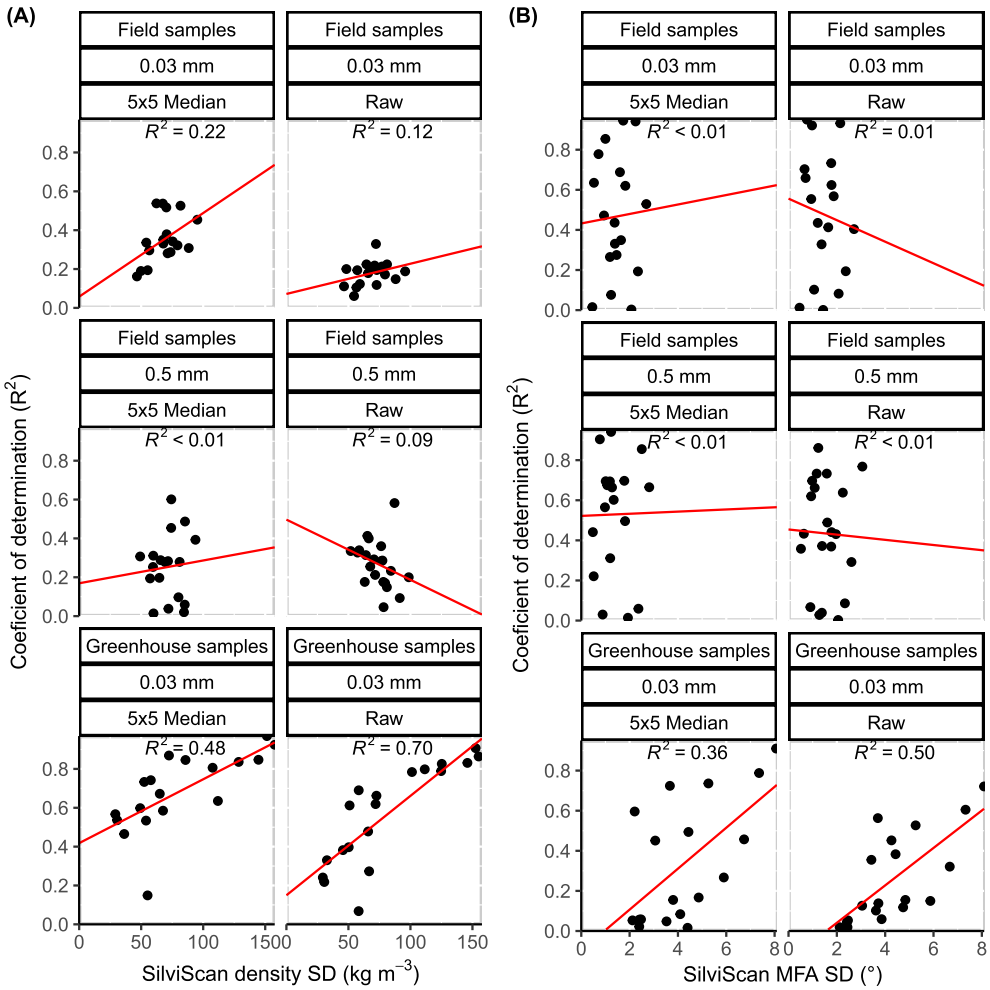

Fig. 3. NIR model performance and the dependency on variation within the samples. (A) Wood density models. (B) MFA models. The dots in (A) and (B) represent the correlation between NIR predicted and reference SilviScan™ data (R^2) in relation to within-sample standard deviation (SD) for the SilviScan™ data. The NIR scans were performed with 0.5 mm or 0.03 mm resolution and with "5 × 5 Median" or "Raw" image processing of samples. The red line shows the best fit linear relationship (n = 18).

samples is the highly juvenile character of wood in the greenhouse samples, often resulting in tension wood formation (wood with lower than normal (<15°) MFA and higher than normal (>500 kg/m^3) wood density) and, hence, higher variation in wood traits. In our samples, the variation in traits such as wood density and MFA were much lower in the field samples than in the greenhouse samples (Fig. 3). Hence, the current wood density model is suitable for juvenile wood from greenhouse-grown trees, but it should be further trained to more accurately detect wood densities in more mature, field-grown trees. However, the model for MFA showed good performance even in samples with low MFA variation (Fig. 3B) and is therefore useful for all sample types tested.

NIR models for wood chemistry

NIR models were created for the relative contents of carbohydrates, total lignin, syringyl-type (S) lignin, guaiacyl-type (G) lignin, *p*-hydroxyphenyl (H) lignin and S/G ratio (Table 1), using reference material analyzed with Py-GC/MS. The obtained R^2 values were 0.78 for carbohydrates, 0.79 for total lignin, 0.58 for S-lignin, 0.74 for G-lignin, 0.84 for H-

lignin, and 0.66 for S:G ratio (Table 1). The NIR model for total lignin (R^2 = 0.79) performed somewhat better than the earlier reported total lignin models (Jones *et al.* 2006; Poke & Raymond 2006) and similar to a model for Klason lignin, where 78% of the variation in the test set was explained by the model (Thumm *et al.* 2016). However, these models were calibrated using wet chemistry methods, hydrolyzing ground wood powder, and measuring acid insoluble and soluble lignin fractions. Also, the earlier models (Jones *et al.* 2006; Poke & Raymond 2006) were based on relatively uniform material in terms of only including trees that were 14 years and older. The satisfactory performance of our models could be related to the high variability in the data due to the presence of tension wood and young trees and to the use of high-resolution sampling of the reference material, enabled by the high-spatial resolution of the Py-GC/MS reference data.

As shown for the wood physical properties, variation within and between samples was important for the training and performance of the NIR models. The average within-sample standard deviation (SD) for both lignin and carbohydrates in greenhouse samples tended to decrease, but not significantly, when the median filter was used (Table 3). However, there was a significant difference in SD between the field and greenhouse samples. The SD for lignin varied from 5.87 to 6.72 in greenhouse samples and from 2.37 to 2.65 for field samples scanned at 0.5-mm resolution, and for carbohydrates from 4.93–5.57 to 2.08–2.36, respectively. The increased variation in the chemical properties of the greenhouse samples compared to the field samples is similar to what was observed for the physical properties and is likely due to the common occurrence of tension wood in the greenhouse samples. An example of the NIR carbohydrate model, mapped on both greenhouse- and field samples, can be seen in Fig. 4.

The carbohydrate content varied a lot within the samples (Fig. 4). Also, the levels of total lignin and the three monolignols varied within the samples (Fig. 5). Interestingly, the level of *p*-hydroxyphenyl appeared higher in areas where the syringyl and guaiacyl levels were relatively low (Fig. 5D). H-lignin distribution is relatively unexplored; at a cellular level it has been shown to occur mainly in the compound middle lamella (Fukushima & Terashima 1990; Simon *et al.* 2018). The relative levels of H-lignin, in bulk samples, have been shown to increase with NO_3^- additions (Renström *et al.* 2024) and have also been referred to as "stress lignin" (Cesarino 2019), prompting further investigations into monolignol biosynthesis in various stages of wood formation. We provide here a method where aspects like monolignol distribution can be studied on a tissue level in response to various developmental and environmental stimuli.

Table 3. The variation within samples for NIR predicted lignin and carbohydrate content and the effect of the median image filter.

Sample type	Resolution	Image filter	Chemical component	Average within sample SD	Tukey
Greenhouse	0.03	Raw	L	6.72	a
Greenhouse	0.03	5 × 5 median	L	5.87	a
Field trial	0.5	5 × 5 median	L	2.65	b
Field trial	0.5	Raw	L	2.37	b
Greenhouse	0.03	Raw	C	5.57	a
Greenhouse	0.03	5 × 5 median	C	4.93	a
Field trial	0.5	5 × 5 median	C	2.36	b
Field trial	0.5	Raw	C	2.08	b

The statistical significance between the SD values was tested with ANOVA and Tukey's Post Hoc test, with different letters (in the "Tukey" column) indicating statistically significant differences. α = 0.05. n = 5–6.

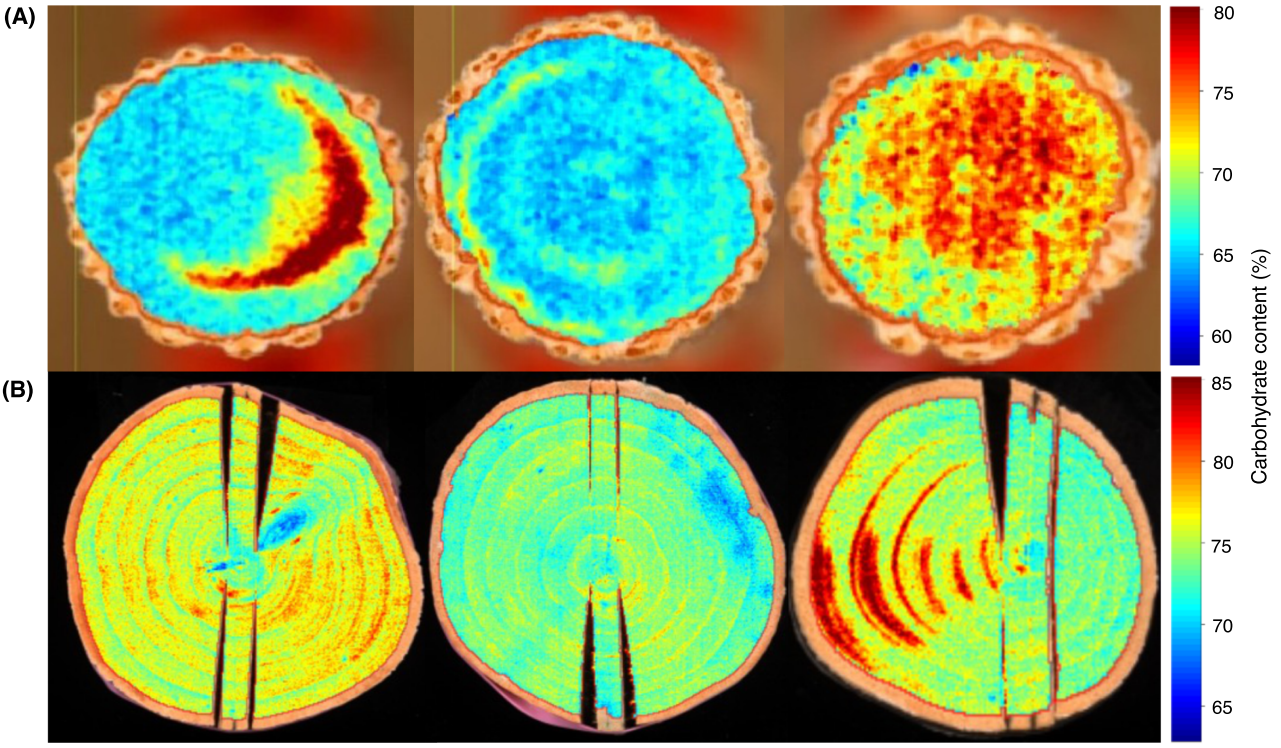

Fig. 4. Examples of the NIR predicted distribution of the carbohydrate fraction in transverse surfaces of wood discs. (A) Greenhouse stems. (B) Field-trial stems with multiple annual rings. The cuts in the field-trial discs were made to avoid uncontrolled cracking while drying. Seasonal variations are clearly visible in stems with multiple annual rings. Py-GC/MS data was used as reference data where carbohydrates constitute both cellulose and hemicelluloses and are presented as an area percentage of the chromatogram. An image filter was applied to reduce noise in the high-resolution images.

NIR model for tension wood

A suitable application of hyperspectral imaging is to detect abnormalities in wood. Others have used the method for detection and classification of the severity of compression wood in softwood species such as *Picea abies* (Duncker & Spiecker 2009) and *Pinus radiata* (Meder & Meglen 2012). Similarly, we constructed an NIR model for the quantification of tension wood based on data from both field- and greenhouse-grown trees. These trees were either subjected to a static bending force or tilted during the growth period to induce the formation of tension wood. Tension wood is often shown to have higher wood density and lower MFA in comparison to normal wood (Hughes 1965; Washusen *et al.* 2001; Coutand *et al.* 2004). Similarly, our SilviScan™ data on the greenhouse samples showed that wood with lower than normal (<15°) MFA had higher than normal (>500 kg/m^3) density (Fig. 2). Therefore, we used the SilviScan™ measurements of MFA and wood density as well as microscopy images to create the model for tension wood probability. The resulting model predicts tension wood probabilities from 0 to 1 in each pixel of an image of a transverse surface. An example image, created by the NIR model, reveals considerable variation in the presence of tension wood on a transverse surface of a greenhouse sample (Fig. 6A). Furthermore, the presence of tension wood coincides with the presence of high NIR-estimated carbohydrate content (Fig. 6B), which is consistent with the higher proportion of cellulose in tension wood compared to normal wood (Timell 1969; Fagerstedt *et al.* 2014). The most frequently observed NIR-estimated carbohydrate level in this image is 69.25% (Fig. 6C), a value that is well within the range of normal wood in *Populus* (Escamez *et al.* 2023; Renström *et al.* 2024). A part of the image shows, however, values over 80% (Fig. 6C), resulting in non-normal distribution of carbohydrate content in the whole

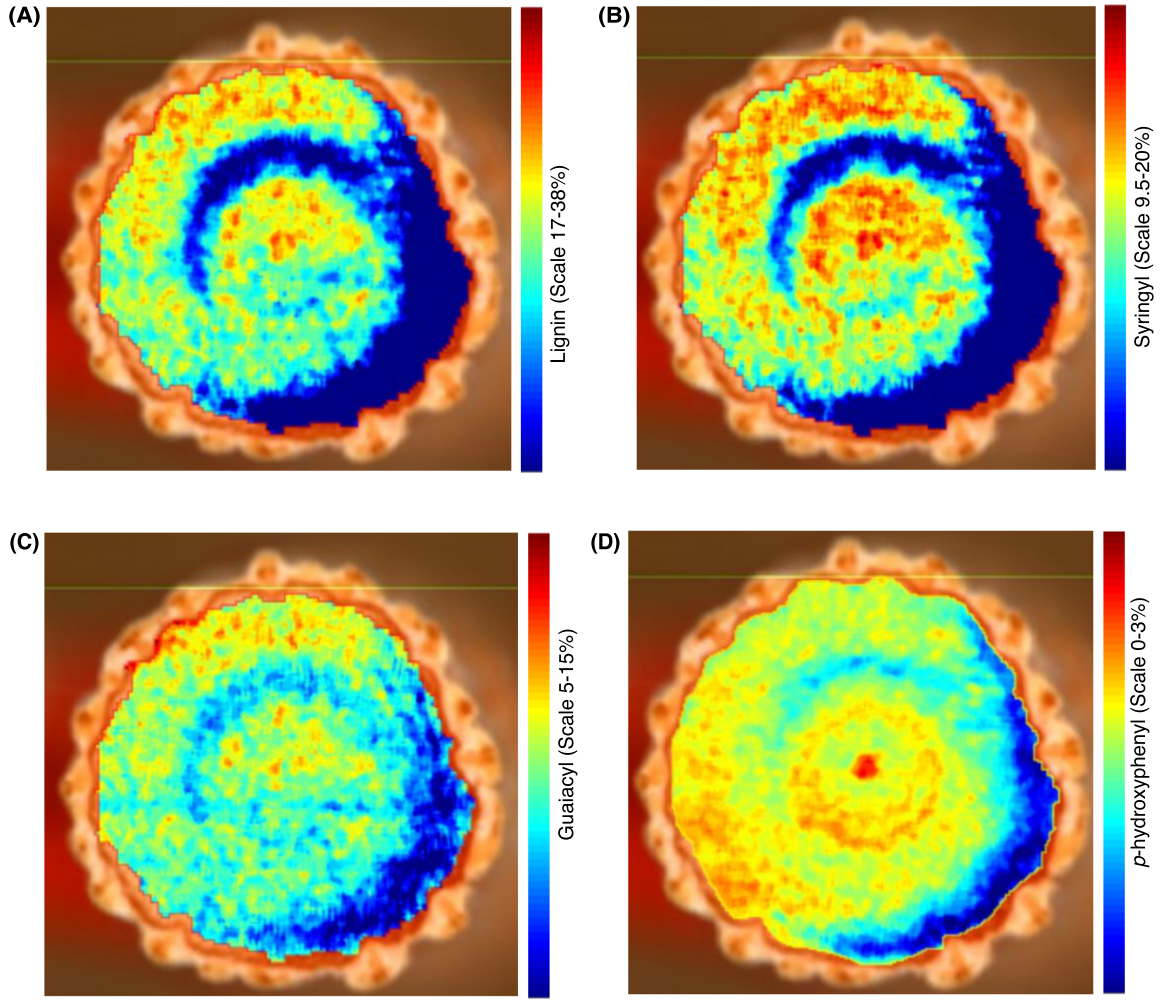

Fig. 5. Median filtered NIR predictions of lignin content and composition in the transverse area of a greenhouse sample. (A) Total lignin. (B) Syringyl lignin units. (C) Guaiacyl lignin units. (D) *p*-hydroxyphenyl lignin units.

transverse surface. The presence of tension wood is, therefore, likely to impact the average values of wood properties such as carbohydrate content, wood density, and MFA. Taken together, variation in wood formation, in particular due to tension wood, demonstrates the importance of spatial imaging of wood chemical and physical properties.

Wood properties of transverse sections versus bulk samples

To evaluate how well the NIR predicted properties on a transversal stem section reflected the bulk properties of the same trees, we used material from greenhouse-grown hybrid aspen trees cultivated under different regimes of nitrogen fertilization (Renström *et al.* 2024).

For wood chemistry, there was a significant correlation between the NIR predicted average of the transverse wood area and the Py-GC/MS determined bulk chemistry data (Fig. 7A). However, for wood density, no correlation was observed between the NIR predicted average of the transverse wood area and the gravimetrically determined bulk data (Fig. 7B).

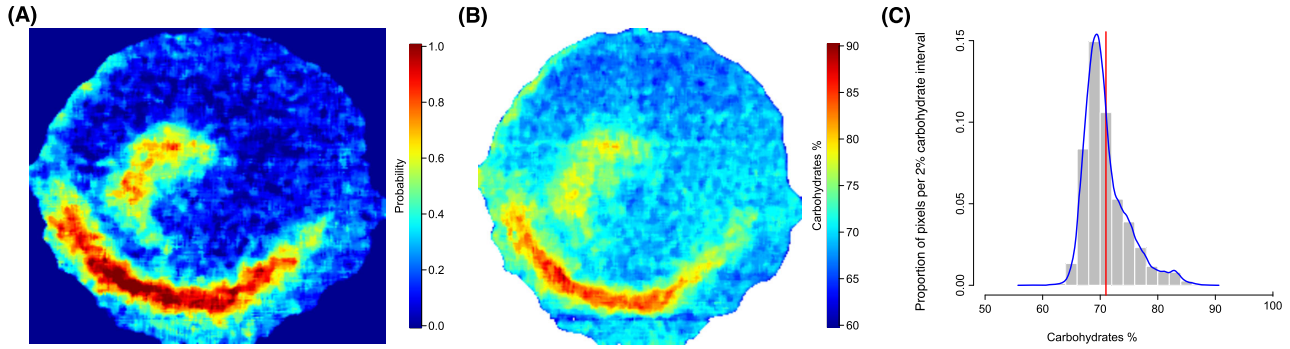

Fig. 6. Tension wood probability prediction with NIR in the stem of a greenhouse sample. (A) Tension wood probability map over the transversal wood area. The scale is 0 to 1, dark blue to dark red, showing a low to high probability of tension wood being present. (B) NIR predicted carbohydrate map of the same transversal area. (C) The corresponding histogram of the NIR predicted carbohydrate fraction (%) in each pixel. The histogram shows the proportion of pixels at 2% carbohydrate intervals. The blue curve shows the probability distribution, and the red line represents the mean value.

Since the content of tension wood in homogenized bulk samples is almost impossible to measure, we cannot provide direct comparisons between the bulk samples and the measurements of the transversal sections. Meanwhile, the correlation between the carbohydrate model and the tension wood model (Fig. 6) suggests that the tension wood model of the transverse sections might also predict the overall content of tension wood in a larger area of the stem. We therefore predicted the tension wood probabilities in the greenhouse samples treated with various nitrogen sources and levels. The probability of tension wood presence was significantly lower in the optimal nitrate (NO_3) treatment compared to the optimal arginine (ARG) treatment (Fig. 7C). In accordance with the lower tension wood content, also the bulk carbohydrate fraction was significantly lower in response to nitrate (Fig. 7D). Tension wood is normally induced as a response to gravitational or mechanical stimulus of the stem (Urbancsok *et al.* 2023). Thus, we suggest that the changes in the wood chemical composition, induced by nitrogen fertilization treatments, could influence the mechanosensitivity of the trees and the occurrence of tension wood in tree stems.

We show here that a single transverse section can provide enough chemical information to estimate wood properties in adjacent stem tissues. The correlation between the carbohydrate and tension wood models, together with the fact that the chemistry models can be used to predict bulk-sample-properties, suggests that NIR predictions of tension wood in a transverse surface can also give information about the presence of tension wood in the corresponding bulk sample.

Conclusions

A high-throughput NIR method is presented for a combined physical and chemical imaging of the whole transversal area of tree stems. We generated NIR models for the physical properties of wood with a resolution of 0.03 mm, which is significantly lower than previously reported. Another significant improvement was the successful analysis of small-diameter stems, and we show in applied examples the suitability of the method for wood characterization of greenhouse-grown trees exposed to various experimental conditions. This study also highlights the challenges in matching spectral and wood property data and the importance of extensive training of the models with high resolution for both the reference data and the NIR images to obtain good prediction accuracies.

We also present a separate model for tension wood, which complements the physical and chemical characterization by informing on the distribution of tension wood within a transverse section. The overlap between the tension wood model and the carbohydrate model demonstrates the robustness of our analyses considering that the reference

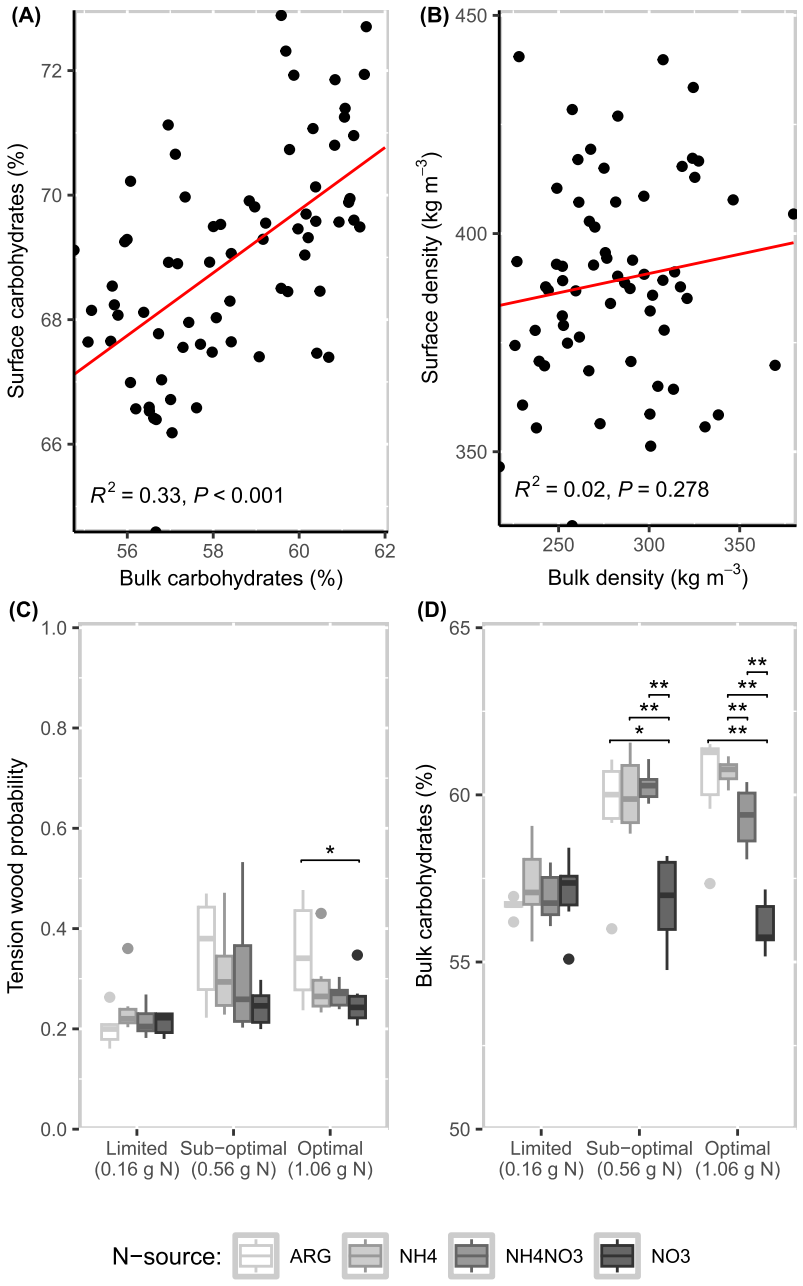

Fig. 7. Wood properties of transverse sections versus bulk samples. (A) Correlation between the average carbohydrate content of bulk samples and the NIR predicted carbohydrate fraction in the transversal area of the stem from the same trees. (B) Correlation between the wood density measured by the water displacement method from a stem piece and the average NIR predicted wood density of the transversal stem section. (C) Tension wood probability in stems of trees cultivated in four different nitrogen sources at three different nitrogen addition levels. (D) Carbohydrate content in wood bulk samples from trees grown in four different nitrogen sources at three different nitrogen addition levels. Boxplots show the distribution of data, 25th, 50th and 75th quartiles, and potential outliers. Statistical significance was tested with the Wilcoxon rank sum test. $\alpha = 0.05$, $n = 6$.

data for these two models were obtained from different sources, i.e. the SilviScan™ and the Py-GC/MS data, respectively.

The spatially resolved sampling for the chemical determination with Py-GC/MS was crucial for producing the corresponding NIR models. We report here for the first time NIR models for lignin monomers. Such models are especially useful for the detection of not only spatial variation in wood chemistry but also temporal regulation of cell wall biosynthesis. In addition, they provide tools to study chemical distribution in response to various developmental and environmental stimuli. For example, the changing climate is known to influence the properties of wood, which can be monitored by high-resolution imaging methods such as the one presented in this paper.

Acknowledgements

We acknowledge Junko Takahashi Schmid at the Biopolymer Analytical Platform (BAP) at UPSC/SLU (supported by Bio4Energy and TC4F) for her help with Py-GC/MS analyses. The work was funded by the Swedish Research Foundation Formas (grant 2021–00992), Bio4Energy (grant B4E3-FM-2-06), and the Knut and Alice Wallenberg (KAW) Foundation (2020.0240). The project was conceived by GS and EJM. EJM, TN, AR and HT provided material for the different analyses and contributed to the pyrolysis-GC/MS analyses. GS, TG and ZY prepared the samples and developed the processing pipeline and the NIR models. EJM and PS identified tension wood used as reference data for the calibration of NIR tension wood models. GS and AR worked on the first draft, and all authors contributed to the writing.

References

Alves A, Cisneros EF, Balmelli G, Poltri SNM, Rodrigues J. 2021. Assessment of eucalypts wood lignin content by analytical pyrolysis, comparison with Klason and total lignin contents. *J. Wood Chem. Technol.* 41(6): 229–235. DOI: 10.1080/02773813.2021.1986071.

Cesarino I. 2019. Structural features and regulation of lignin deposited upon biotic and abiotic stresses. *Curr. Opin. Biotechnol.* 56: 209–214. DOI: 10.1016/j.copbio.2018.12.012.

Cieszewski CJ, Strub M, Antony F, Bettinger P, Dahlen J, Lowe RC. 2013. Wood quality assessment of tree trunk from the tree branch sample and auxiliary data based on NIR spectroscopy and silviscan. *Math. Comput. For. Nat.-Resour. Sci.* 5(1): 86–111.

Coutand C, Jeronimidis G, Chanson B, Loup C. 2004. Comparison of mechanical properties of tension and opposite wood in Populus. *Wood Sci. Technol.* 38: 11–24. DOI: 10.1007/s00226-003-0194-4.

Duncker P, Spiecker H. 2009. Detection and classification of Norway spruce compression wood in reflected light by means of hyperspectral image analysis. *IAWA J.* 30(1): 59–70. DOI: 10.1163/22941932-90000203.

Erasmus J, Drew DM, du Toit B, Wessels CB. 2020. *Modelling the effect of stand density management and environmental variables on Pinus patula wood properties: The effect of water supply and Nitrogen/Potassium ratio on selected wood properties of Pinus patula, Pinus elliottii × caribaea, and Pinus patula × tecunumanii saplings Doctoral thesis*. Stellenbosch University, Stellenbosch, available online at http://hdl.handle.net/10019.1/108025.

Escamez S, Latha Gandla M, Derba-Maceluch M, Lundqvist SO, Mellerowicz EJ, Jönsson LJ, Tuominen H. 2017. A collection of genetically engineered *Populus* trees reveals wood biomass traits that predict glucose yield from enzymatic hydrolysis. *Sci. Rep.* 7(1): 1–11. DOI: 10.1038/s41598-017-16013-0.

Escamez S, Robinson KM, Luomaranta M, Gandla ML, Mähler N, Yassin Z, Grahn T, Scheepers G, Stener LG, Jansson S, Jönsson LJ, Street NR, Tuominen H. 2023. Genetic markers and tree properties predicting wood biorefining potential in aspen (*Populus tremula*) bioenergy feedstock. *Biotechnol. Biofuels Bioprod.* 16(1): 1–16. DOI: 10.1186/s13068-023-02315-1.

Evans R. 1994. Rapid measurement of the transverse dimensions of tracheids in radial wood sections from *Pinus radiata*. *Holzforschung* 48(2): 168–172. DOI: 10.1515/hfsg.1994.48.2.168.

Faber NM. 1999. Estimating the uncertainty in estimates of root mean square error of prediction: application to determining the size of an adequate test set in multivariate calibration. *Chemometr. Intell. Lab. Syst.* 49(1): 79–89. DOI: 10.1016/S0169-7439(99)00027-1.

Fagerstedt KV, Mellerowicz E, Gorshkova T, Ruel K, Joseleau J-P. 2014. Cell wall polymers in reaction wood. In: Gardiner B, Barnett J, Saranpää P, Gril J (eds.), *The Biology of Reaction Wood*: 37–106. Springer, Berlin, Heidelberg.

Fahey LM, Nieuwoudt MK, Harris PJ. 2019. Predicting the cell-wall compositions of solid *Pinus radiata* (radiata pine) wood using NIR and ATR FTIR spectroscopies. *Cellulose* 26(13–14): 7695–7716. DOI: 10.1007/s10570-019-02659-8.

Fukushima K, Terashima N. 1990. Heterogeneity in formation of lignin. XIII. Formation of p-hydroxyphenyl lignin in various hardwoods visualized by microautoradiography. *J. Wood Chem. Technol.* 10(4): 413–433. DOI: 10.1080/02773819008050250.

Gerber L, Eliasson M, Trygg J, Moritz T, Sundberg B. 2012. Multivariate curve resolution provides a high-throughput data processing pipeline for pyrolysis-gas chromatography/mass spectrometry. *J. Anal. Appl. Pyrol.* 95: 95–100. DOI: 10.1016/j.jaap.2012.01.011.

Giroud G, Bégin J, Defo M, Ung C-H. 2017. Regional variation in wood density and modulus of elasticity of Quebec's main boreal tree species. *For. Ecol. Manage.* 400: 289–299. DOI: 10.1016/j.foreco.2017.06.019.

Giroud G, Defo M, Bégin J. 2021. Determination of radial profiles of wood properties using a near infrared scanning system. *J. Near Infrared Spectrosc.* 29(1): 24–32. DOI: 10.1177/0967033520967324.

Hein PRG. 2012. Estimating shrinkage, microfibril angle and density of *Eucalyptus* wood using near infrared spectroscopy. *J. Near Infrared Spectrosc.* 20(4): 427–436. DOI: 10.1255/jnirs.1005.

Hein PRG, Pakkanen HK, Dos Santos AA. 2017. Challenges in the use of near infrared spectroscopy for improving wood quality: A review. *For. Syst.* 26(3): eR03. DOI: 10.5424/fs/2017263-11892.

Hughes FE. 1965. Tension wood – a review of literature. *For. Abstr.* 26(2): 179–186.

Inagaki T, Schwanninger M, Kato R, Kurata Y, Thanapase W, Puthson P, Tsuchikawa S. 2012. *Eucalyptus camaldulensis* density and fiber length estimated by near-infrared spectroscopy. *Wood Sci. Technol.* 46(1–3): 143–155. DOI: 10.1007/s00226-010-0379-6.

Isik F, Mora CR, Schimleck LR. 2011. Genetic variation in *Pinus taeda* wood properties predicted using non-destructive techniques. *Ann. For. Sci.* 68(2): 283–293. DOI: 10.1007/s13595-011-0035-9.

Jones PD, Schimleck LR, Peter GF, Daniels RF, Clark A. 2006. Nondestructive estimation of wood chemical composition of sections of radial wood strips by diffuse reflectance near infrared spectroscopy. *Wood Sci. Technol.* 40(8): 709–720. DOI: 10.1007/s00226-006-0085-6.

Karmanov AP, Shaposhnikova LM, Kocheva LS, Rachkova NG, Belyy VA, Lutoev V. 2023. Structural features of stress lignin of aspen (*Populus tremula* L.) growing under increased background radiation. *Biocatal. Agric. Biotechnol.* 50: 102677. DOI: 10.1016/j.bcab.2023.102677.

Kusch P. 2018. Introductory chapter: analytical pyrolysis-gas chromatography/mass spectrometry of polymeric materials. In: *Analytical Pyrolysis*: 1–6. IntechOpen eBooks, London. DOI: 10.5772/intechopen.81596.

Meder R, Meglen RR. 2012. Near infrared spectroscopic and hyperspectral imaging of compression wood in *Pinus radiata* D. Don. *J. Near Infrared Spectrosc.* 20(5): 583–589. DOI: 10.1255/jnirs.1001.

Mesquita Pimenta E, Dos Santos Brito EG, Ramalho FMG, Hein PRG. 2024. Validation of models using near-infrared spectroscopy to estimate basic density and chemical composition of *Eucalyptus* wood. *iForest – Biogeosci. For.* 17(6): 338–345. DOI: 10.3832/ifor4516-017.

Mora CR, Schimleck LR. 2009. Determination of within-tree variation of *Pinus taeda* wood properties by near infrared spectroscopy. Part 2: Whole-tree wood property maps. *Appita J.* 62(3): 232–238.

Poke FS, Raymond CA. 2006. Predicting extractives, lignin, and cellulose contents using near infrared spectroscopy on solid wood in *Eucalyptus globulus*. *J. Wood Chem. Technol.* 26(2): 187–199. DOI: 10.1080/02773810600732708.

Preibisch S, Saalfeld S, Tomancak P. 2009. Globally optimal stitching of tiled 3D microscopic image acquisitions. *Bioinformatics* 25(11): 1463–1465. DOI: 10.1093/bioinformatics/btp184.

Renström A, Choudhary S, Gandla ML, Jönsson LJ, Hedenström M, Jämtgård S, Tuominen H. 2024. The effect of nitrogen source and levels on hybrid aspen tree physiology and wood formation. *Physiol. Plant.* 176(1): e14219. DOI: 10.1111/ppl.14219.

Schimleck L, Antony F, Mora C, Dahlen J. 2018. Comparison of whole-treewood property maps for 13- and 22-year-old loblolly pine. *Forests* 9(6): 1–11. DOI: 10.3390/f9060287.

Schimleck LR, Evans R, Jones PD, Daniels RF, Peter GF, Clark A. 2005. Estimation of microfibril angle and stiffness by near infrared spectroscopy using sample sets having limited wood density variation. *IAWA J.* 26(2): 175–187. DOI: 10.1163/22941932-90000109.

Schindelin J, Arganda-Carreras I, Frise E, Kaynig V, Longair M, Pietzsch T, Preibisch S, Rueden C, Saalfeld S, Schmid B, Tinevez JY, White DJ, Hartenstein V, Eliceiri K, Tomancak P, Cardona A. 2012. Fiji: An open-source platform for biological-image analysis. *Nature Methods* 9(7): 676–682. DOI: 10.1038/nmeth.2019.

Simon C, Lion C, Spriet C, Baldacci-Cresp F, Hawkins S, Biot C. 2018. One, two, three: a bioorthogonal triple labelling strategy for studying the dynamics of plant cell wall formation in vivo. *Angew. Chem. Int. Edn.* 57(51): 16665–16671. DOI: 10.1002/anie.201808493.

Thumm A, Riddell M, Nanayakkara B, Harrington J, Meder R. 2016. Mapping within-stem variation of chemical composition by near infrared hyperspectral imaging. *J. Near Infrared Spectrosc.* 24(6): 605–616. DOI: 10.1255/jnirs.1206.

Timell T. 1969. The chemical composition of tension wood. *Svensk Papperstidning* 72: 173–181.

Tsuchikawa S. 2007. A review of recent near infrared research for wood and paper. *Appl. Spectrosc. Rev.* 42(1): 43–71. DOI: 10.1080/05704920601036707.

Urbancsok J, Donev EN, Sivan P, van Zalen E, Barbut FR, Derba-Maceluch M, Šimura J, Yassin Z, Gandla ML, Karady M. 2023. Flexure wood formation via growth reprogramming in hybrid aspen involves jasmonates and polyamines and transcriptional changes resembling tension wood development. *New Phytol.* 240(6): 2312–2334. DOI: 10.1111/nph.19307.

Washusen R, Ades P, Evans R, Ilic J, Vinden P. 2001. Relationships between density, shrinkage, extractives content and microfibril angle in tension wood from three provenances of 10-year-old *Eucalyptus globulus* Labill. *Holzforschung* 55(2): 176–182. DOI: 10.1515/HF.2001.029.

Edited by Lloyd Donaldson

Supplementary material

Table A1. Raw data for comparison of bulk versus NIR predicted surface properties for wood density and chemical composition. This table can be accessed at 10.6084/m9.figshare.28322243.